Available online at www.sciencedirect.com

ScienceDirect

Energy Procedia 142 (2017) 809–814

Energy Procedia

www.elsevier.com/locate/procedia

9th International Conference on Applied Energy, ICAE2017, 21-24 August 2017, Cardiff, UK

Experimental characterization and multi-physics simulation of a triple-junction cell in a novel hybrid III:V concentrator photovoltaic–thermoelectric receiver design with secondary optical element

T K N Sweet[a*], M H Rolley[a], W Li[b], M C Paul[b*], M Gao[a] and A R Knox[b]

[a]*School of Engineering, Cardiff University, Cardiff. CF24 3AA, UK*
[b]*School of Engineering, University of Glasgow, Glasgow, G12 8QQ, UK*

Abstract

A lattice-matched monolithic triple-junction Concentrator Photovoltaic cell ($InGa_{(0.495)}P/GaIn_{(0.012)}As/Ge$) was electrically and thermally interfaced to a Thermoelectric Peltier module. A single optical design secondary lens was bonded to the CPV-TE receiver. The hybrid SILO-CPV-TE solar energy harvesting device was electrically, thermally and theoretically investigated. The electrical performance data for the cell under variable irradiance and cell temperature conditions were measured using the integrated thermoelectric module as both a temperature sensor and as a solid-state heat pump. The cell was electrically characterised under standard test conditions (1000 W/m^2 irradiance, 25^{o}C temperature and AM1.5G spectrum) for comparison with literature data. Transient multiphysics simulations in ANSYS CFX 15.0 were carried out to calculate cell temperatures and to determine the short circuit current and temperature coefficient in a scaling law. The optimization was used to determine 15 model parameters for the component sub-cells within the triple-junction cell at STC with a MATLAB scaling law. The root-mean-square error in electrical currents between measurement and simulations was 0.66%.

Peer-review under responsibility of the scientific committee of the 9th International Conference on Applied Energy.

Keywords: Concentrator photovoltaic; triple-junction solar cell; thermoelectric; cell temperature; secondary optical element; optimization

1. Introduction

Concentrator photovoltaic technology (CPV) is a viable option for commercial-scale generation of solar electricity in areas of high direct normal irradiance (DNI >2000 kWh/m^2). Cumulative global installation capacity of CPV

* Corresponding authors. Tel.: +44(0)2920870673 and +44(0)141 330 8466; fax: +44(0)141 330 2032.
E-mail addresses: SweetT@Cardiff.ac.uk; Manosh.Paul@Glasgow.ac.uk

1876-6102
Peer-review under responsibility of the scientific committee of the 9th International Conference on Applied Energy.
10.1016/j.egypro.2017.12.130

exceeds 370MWp (Dec 2016) [1]. Low cost glass or polymer concentrating optics are used to significantly increase photon flux onto a small [typically 5.5mm x 5.5mm] CPV cell. The optics concentrate sunlight (between 300x and 1000x) and homogenize photon spectral distribution, increasing cell efficiency. CPV is competitive with flat-plate crystalline Silicon Photovoltaic (PV) technologies in terms of levelized costs of electricity (LCoE) in high DNI locations. Modular CPV systems typically include dual-axis tracking systems to follow the sun's trajectory and maximize energy generation throughout the day. A significant benefit of CPV is the comparatively high cell, and therefore system, efficiencies produced. Compound semiconductor CPV cells are structurally designed to minimize thermalisation and transmission losses. Multiple direct bandgap materials are epitaxially grown via metal organic vapour phase epitaxy (MOVPE) or molecular beam epitaxy (MBE). High purity III:V layers, with typical total thickness of <10μm, have almost perfect crystallinity leading to low non-radiative losses in the CPV device. High extinction coefficients and anti-reflective coating of the cell enables effective absorption of incident solar photons in the wavelength range, 250-2500nm. High charge carrier mobility and separation enables full-spectrum energy harvesting. Currently the world record efficiency for a multi-junction solar cell is 46.0% by Fraunhofer ISE, Soitec and CEA-LETI [1, 2]. World III:V cell efficiency records have typically increased ~1% per year over the past decade. Advanced modelling indicates realistic cell efficiency targets of greater than 50% (1000x concentration) by 2020[3]. High-volume production cell efficiencies closely follow this trend.

To maximize optical concentration two lenses are typically applied, a primary optical element (POE) and a secondary optical element (SOE). A domed-shaped SIngLe Optical (SILO) lens, which also encapsulates the CPV cell, was used as the SOE in this work [4]. An inevitable consequence of high irradiance conditions is elevated cell temperatures and net power reduction. The bandgap of each photon-absorbing layers is altered [5] reducing the cell voltage and slightly increasing photo-generated current. The thermoelectric (TE) module in the hybrid CPV-TE receiver was used as both a cell temperature sensor (via V_{oc}) and a heat pump (upon application of current). Active solid-state cooling of the CPV cell increased power output and reduced thermal degradation of the semiconductor. The novel hybrid SILO-CPV-TE receiver was electrically and thermally measured under different irradiance and cell temperature conditions. Standard test conditions (STC) of 1000W/m^2 irradiance, 25^{o}C temperature and AM1.5G spectrum conditions gave baseline cell performance data. Multiphysics simulation techniques were used to predict the time-dependent cell temperature based on the recorded indoor ambient temperature and TE measurements. The electric performance of the triple-junction cell based CPV system was then modelled.

2. Experimental.

The SILO-CPV-TE receiver was manufactured using standard cleanroom and wire-bonding techniques. The architecture of the hybrid device is given in Fig 1(a) [5]. The active components consisted of a 5.5×5.5mm lattice-matched triple junction CPV cell bonded to a Marlow CM23-1.9 bismuth telluride TE module. A photograph of the receiver showing electrical contacts, Fig 1(b) includes a water heat exchanger and appropriate thermal interface material (TIM). Temperature measurements were taken (TE cold-side and ambient) with K-type thermocouples connected to a Fluke 52II thermometer. Additionally a Closed Loop Integrated Cooler (CLIC) temperature reference chip (Temp IC) gave temperature data alongside a forward looking infrared camera (FLiR i7) for thermal imaging measurements.

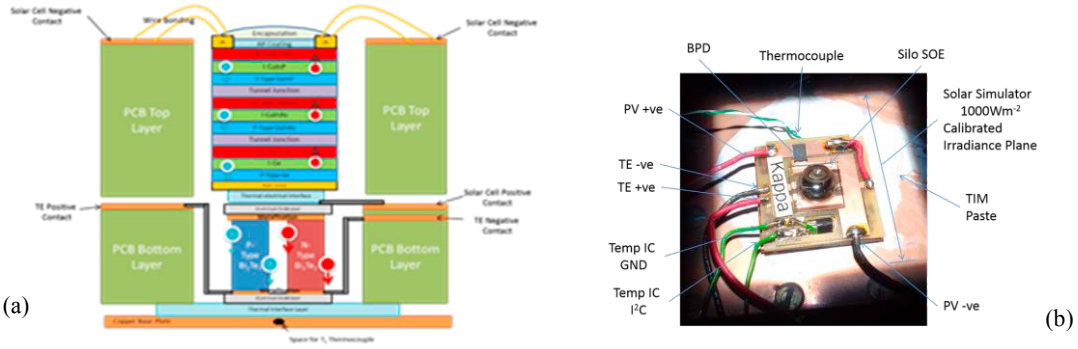

Fig.1 (a) Cross-section of the CPV-TE receiver and (b) Kappa SILO-CPV-TE hybrid receiver overview.

A LCS-100 Class ABB (ASTM, IEC and JIS standards) solar simulator, with the 1000W/m^2 calibrated irradiance plane found using a Kipp and Zohan CMP11 pyranometer, was used for current-voltage (I-V) scans. An AUTOLAB potentiostat system was used for I-V data acquisition, and the experiments were conducted inside a Faraday cage to eliminate any ambient light effects, see Fig 2. Steady-state temperatures were achieved, prior to measuring solar cell I-V curves, to eliminate changes in electrical output due to the temperature coefficient effects of the solar cell.

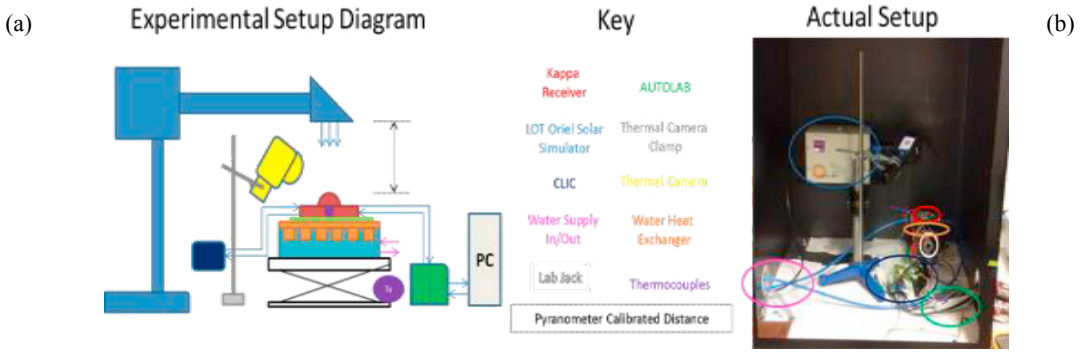

Fig.2 (a) Overview of the experimental setup and (b) actual experimental setup in the Faraday cage.

3. Simulation

The computational domain consisted of a body of air between the solar simulator aperture (57mm×38mm) and the dome lens, the dome lens itself, the cell and a thermal interface material (TIM) layer between the cell and the TE module surface, as shown in Fig.3. The air body volume was defined as 57mm×38mm×159.7mm. The dome lens height was measured 10mm from apex to base. The cell (5.5×5.5mm) in Fig. 1 was simplified as one layer using an equivalent heat transfer property constant, calculated using 1D elementary conductive heat transfer formula [6]. The CFD package-ANSYS CFX 15.0 was used to carry out transient multi-physics simulations. The transient laminar fluid flow governing equations chosen were the Boussinesq approximation, natural convective heat transfer equations and grey radiative models. These were incorporated to describe the buoyancy-driven air flow between the solar aperture and the dome lens to investigate influence on cell temperature. The conductive heat transfer equations and grey radiative models were used for the dome lens and cell, while the conductive heat transfer equations were applied to the TIM layer. The fluid flow, convective, conductive heat transfer equations were discretized using a finite volume method. Coupling between the continuity and momentum equations was accomplished with the "SIMPLE" algorithm. The grey radiative equation was solved by means of a Monte Carlo method. The air body, and dome lens were discretized with tetrahedral elements. The cell and TIM layer were discretized with hexahedrons. Three sets of meshes with 112888, 359217 and 1623711 elements respectively. The ambient and TE temperatures recorded during the experiment were input into CFX as a function of time. The average temperatures in the cell and dome lens were recorded by monitor expressions in the CFX Output Control. The 100s time-step in the transient simulations had 100 iterations in each time step, root-mean square residual target 10^{-5}.

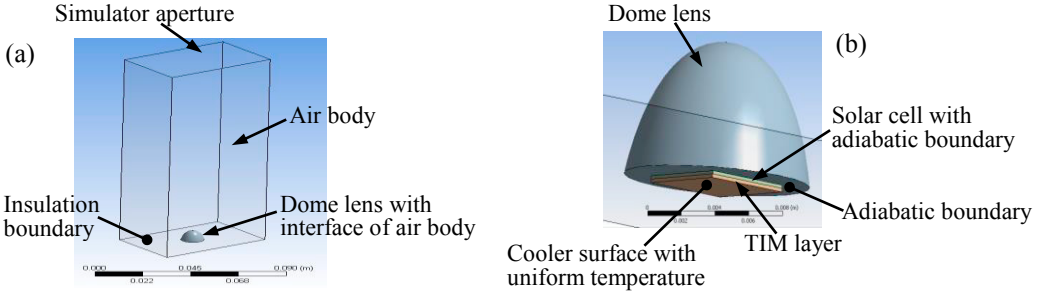

Fig. 3 Computational (a) measurement domain and (b) receiver domain

3.1. Electric model

The effectiveness of a five-parameter scaling law technique has been previously demonstrated on a single junction solar cell [9] and silicon-based modules and arrays [8,9] to obtain off-STC datasets from an STC input. During experimental measurements the cell temperature can deviate from the STC 25ºC at 1000W/m^2 irradiance. Hence, the model described in this paper was used to obtain the critical parameters at 25ºC based on an I-V curve measured at a temperature different to 25ºC. Existing scaling laws for solar cells show that the fifteen solar cell parameters at a temperature different to 25ºC can be found.

The shunt resistance, R_{sh}, series resistance R_s and ideality index n depend on irradiance only. The short circuit current I_{sc} is dependent on both the cell temperature and irradiance whereas the diode reverse saturation current I_d is dependent on cell temperature alone. Therefore, under a constant irradiance, R_{sh}, R_s and n remain unchanged regardless of the cell temperature, but I_{sc} and I_d vary with cell temperature [7,8,9]. In this scenario, the existing scaling law was expressed by equations below (1) where subscript index i=1, 2, 3 was used to denote to the top InGaP cell, middle InGaAs cell and bottom Ge cell respectively, as shown in Fig. 4.

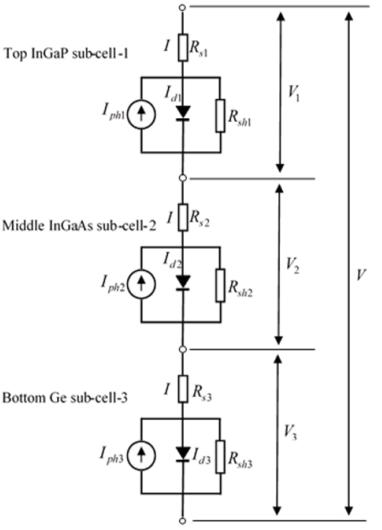

Fig.4 Lumped electric model of 3J cell

$$\begin{cases} n_i = n_{0i}, R_{si} = R_{s0i}, R_{shi} = R_{sh0i} \\ I_{phi} = I_{sc0i} + \mu\left(T - T_0\right) \\ I_{di} = I_{d0i}\left(T/T_0\right)^3 \exp\left[\frac{1}{k}\left(\frac{Eg0i}{T_0} - \frac{Egi}{T}\right)\right], i = 1,2,3 \end{cases} \quad (1)$$

Subscript 0 is the cell operating at 25ºC STC, μ the short-circuit temperature coefficient, 2.2188×10^{-5} A/K based on experimental I-V curves (Fig.5). κ Boltzmann constant, 8.61733035×10^{-5}eV/K. Sub-cell temperature (T) at non STC conditions, $I_{phi} \approx I_{sci}$. The three sub-cells were assumed to share the same temperature. E_{gi} is the band gap of the top InGaP cell [8], middle InGaAs cell [9] and bottom Ge cell [10], respectively. Under STC conditions, the I-V curve of a triple-junction solar cell can be written as (2)

$$\begin{cases} I = \dfrac{\sum_{i=1}^{3} I_{sc0i} R_{sh0i} - \sum_{i=1}^{3} I_{d0i}\left\{\exp\left[\dfrac{q\left(V_i + IR_{s0i}\right)}{n_{0i}\kappa T_0}\right] - 1\right\} R_{sh0i} - V}{\sum_{i=1}^{3}\left(R_{s0i} + R_{sh0i}\right)} \\ V_1 = 0.5V, V_2 = 0.35V, V_3 = 0.15V \end{cases} \quad (2)$$

where q is the electron charge, q =1.60217662 × 10^{-19}C, the Boltzmann constant is κ =1.38064852×10^{-23}J/K. The second equation in Eq. (2) is based on [11]. Under an off STC condition where the cell temperature is no longer equal to 25ºC but the irradiance is kept at 1kW/m^2, the I-V curve of the triple-junction solar cell is expressed as (3)

$$\begin{cases} I = \dfrac{\sum_{i=1}^{3} I_{phi} R_{shi} - \sum_{i=1}^{3} I_{di}\left\{\exp\left[\dfrac{q\left(V_i + IR_{si}\right)}{n_i \kappa T}\right] - 1\right\} R_{shi} - V}{\sum_{i=1}^{3}\left(R_{si} + R_{shi}\right)} \\ V_1 = 0.5V, V_2 = 0.35V, V_3 = 0.15V \end{cases} \quad (3)$$

If the 15 model parameters I_{sc0i} I_{d0i}, R_{s0i}, n_{0i}, R_{sh0i} at STC and the scaling law, Eq. (1), are available, then the 15 model parameters I_{phi} I_{di}, R_{si}, n_i and R_{shi} at different temperatures will be predicted. The off-STC I-V curves can then be calculated. Our task is to determine the 15 model parameters, at STC, from two sets of I-V curves at cell temperatures other than 25ºC. This inverse problem can be expressed mathematically in (4)

$$f\left[I_{sc0i}, I_{d0i}, R_{s0i}, n_{0i}, R_{sh0i}, \text{scaling law of Eq.(1)}\right] = \sum_{j=1}^{N}\left(I_j^m - I_j^e\right)^2 \to \min \quad (4)$$

Where I_j^m and I_j^e are the current predicted with Eq. (4) and the off STC measured current at a voltage V_j^e, j is the index indicating an experimental data point, N is the number of total experimental data points. I_{sc0i} I_{d0i}, R_{s0i}, n_{0i} and R_{sh0i} are determined at STC by trust-region-reflective least squares algorithm (*lsqnonlin function*) in MATLAB. The structural design and epitaxial growth of the three sub-cells are designed to be current-matched, producing simultaneous I-V maximum power point. It was assumed that the three series-connected sub-cells share the same I_{sc0}, thus there are 13 independent variables in the optimization. Further developments could experimentally and theoretically investigate any ratio between I_{sc0} of the sub-cells for model input and test data verification.

4. Results

To accurately estimate CPV cell temperature, a CFX transient multiphysics simulation was done, using a representative thermal contact resistance 20cm^2 s K/cal (4.7801×10^{-4}m^2 K/W) at the cell – TIM layer interface. Using this correction, the temperature profile showed better agreement (Fig.5). Under this thermal contact resistance, the mean cell temperature was found to be 14.86ºC at a time of 60min. Each of the three meshes computed above, represent different resolutions of the ANSYS calculated cell temperature. The temperature given by mesh 1 shows a large error being 1.82% lower than mesh two. The two higher resolution meshes agreed within 0.8%. The cell temperature from mesh 2 was chosen (14.59ºC), due to the negligible temperature deviation of mesh 2 and 3, combined with a consideration for optimal computation time of the model. The temperature coefficient of short current of the cell was then calculated μ, i.e., $\mu=(I_{sc2}-I_{sc1})/(T_2-T)$, where I_{sc1}=9.9550×10^{-3}A and I_{sc2}=9.7930×10^{-3}A at T_1=22.2 and T_2=14.59ºC. With these data, the temperature coefficient can be worked out as μ=2.1288×10^{-5} A/K.

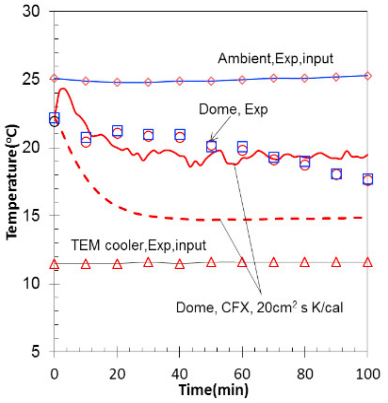

Fig.5 Input and output temperature profiles

$$\mu=\frac{I_{sh2}-I_{sh1}}{T_2-T_1} \tag{6}$$

The I-V curves at two cell temperatures T_1=22.2 ºC and T_2=14.59ºC were experimentally measured. Curves were fitted to extract 15 electric model parameters at STC. Appropriate boundary conditions were used for the calculation of each parameter by referring to existing results of similar triple-junction cells [12]. The extracted parameters, Table 1 and Fig 6, have a calculated root-mean-square error (RMSE) of 0.66%.

.

Table 1 Model calculated parameters of three sub-cells at STC from an off-STC input.
The predicted currents at two cell temperatures are compared against experimental data (normalized using mean experimental Isc).

Parameter	R_{s0i} (Ω)	R_{sh0i} (Ω)	n_{0i}	I_{d0i} (μA)	I_{sc0i} (A)	RMSE (%)
Top InGaP cell, i =1	2.6862×10^{-4}	7.0745×10^3	2.0942	9.2988×10^{-6}	1.0089×10^{-2}	0.66
Middle InGaAs cell, i =2	2.6383×10^{-5}	1.8058×10^2	3.8663	6.4962×10^{-6}	1.0089×10^{-2}	
Bottom Ge cell, i =3	3.9090×10^{-4}	1.8011×10^2	4.6264	3.1829×10^{-6}	1.0089×10^{-2}	

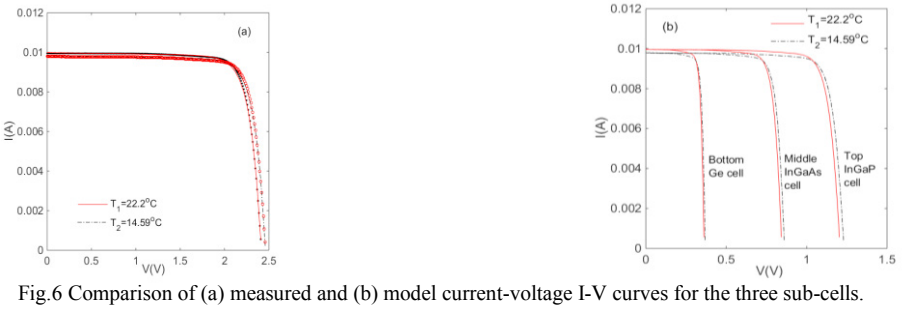

Fig.6 Comparison of (a) measured and (b) model current-voltage I-V curves for the three sub-cells.

5. Conclusions

Novel hybrid SILO-CPV-TE receivers were manufactured and electrically, thermally and theoretically analysed. The integrated TE module successfully acted as both a temperature sensor and as a solid-state heat pump for the CPV cell. This experimental platform enables accurate measurement of electrical current-voltage characteristics under standard test conditions (1000W/m^2 irradiance, 25^{o}C temperature and AM1.5G spectrum).

A method for determining 15 parameters of the three component sub-cells in an InGaP/InGaAs/Ge triple-junction solar cell at STC, using experimental input data has been presented. Experimental I-V curves obtained in a solar simulator at STC and non-STC temperatures at 1000W/m^2 irradiance were used for ANSYS CFX 15.0 model validation, calibration and performance evaluation. The CPV cell temperature, short circuit current and temperature co-efficient within the hybrid device were calculated via a scaling law in the multi-physics simulations. The method was successfully coded in MATLAB and the 15 parameters for the component sub-cells were optimized/extracted at STC. A small error at the I-V curve 'knee', the location near the Maximum Power Point, is caused from the one-diode model adopted here. Overall the RMSE for electrical currents was shown to be 0.66% for all three sub cells, showing excellent curve fitting and validation of both the experimental methodology and the simulation model.

Future work will include installation of a primary optical element for higher optical concentration and further development of automatic sampling. The multi-physics model presented also shows potential for modification/development to analyse band gap changes related to changes in the incident solar spectrum on the CPV cell. The experimental and theoretical work presented in this paper can be used for further thermally-dependant CPV cell characterisation (both STC and non-STC) conditions. This data will be used for future hybrid CPV-TE device architectures to optimise electrical performance and device/system lifetime whilst minimising levelised cost of energy at system level.

Acknowledgements

Sêr Cymru National Research Network and the EPSRC Solar Challenge project SUNTRAP (EP/K022156/1) are gratefully acknowledged for financial support. Grateful thanks are extended to IQE plc for supply of high efficiency III-V triple-junction CPV cells, and Cardiff University School of Physics for the use of cleanroom facilities.

References

[1] Green MA, Emery K, Hishikawa Y, Warta W and Dunlop ED, Solar cell efficiency tables (version 47), Prog. Photovolt., Res. Appl., 24 (1), 3-11, 2016.
[2] Dimroth F, Tibbits TND, Niemeyer M, et al, Four-junction wafer-bonded concentrator solar cells, IEEE J. Photovolt., 6 (1) 343-349, 2016.
[3] Lumb M et al, 43rd PVSEC 2016 [http://www.pvsec-26.com/pvsec-2016-singapore]
[4] James LW, Sandia National Laboratories Albuquerque, New Mexico for US Department of Energy (SAND89-7029), 1989.
[5] Sweet TKN, Rolley M, Min G, et al, Scalable solar thermoelectric and photovoltaics (SUNTRAP), American Institute of Physics, 1766, 080007, 2016.
[6] Incropera FP, Dewitt DP, Bergman TL and Lavine AS, Fundamentals of Heat and Mass Transfer, 6tt edition, Hoboken: John Willey & Sons, 2007
[7] De Soto W, Klein SA, Beckman WA, Improvement and validation of a model for photovoltaic array performance, Solar Energy, 80, 78-88, 2006.
[8] Dongue S, Njomo D, Ebengai L, An improved nonlinear five-point model for photovoltaic modules, International Journal of Photoenergy, 11 pages, 2013.
[9] Siddiqui MU, Arif AFM, Kelly L, Dubowsky S, Three-dimensional thermal modelling of a photovoltaic module under varying condition, Solar Energy, 86, 2620-2631, 2012.
[10] O'Donnell K P and Chen X, Temperature dependence of semiconductor band gap, Applied Physics Letters, 58(25), 2924-2926, 1991.
[11] Ben Or A and Appelbaum J, Estimation of multi-junction solar cell parameters, Progress in Photovoltaics: Research and Applications, 21, 713-723, 2013.
[12] Wei J, Murray JM, Barnes J, Gonzalez L P, Guha S, Determination of the temperature dependence of the band gap energy of semiconductors from transmission spectra, Journal of Electronics Materials, 41(10), 2857-2866, 2012.